Pulse dynamics controlled by saturable absorber in a dispersion-managed normal dispersion Tm-doped mode-locked fiber laser

Xiaoliang Yang (杨小亮), Yu Chen (陈 宇), Chujun Zhao (赵楚军)*, and Han Zhang (张 晗)

Key Laboratory for Micro-/Nano-Optoelectronic Devices of Ministry of Education, College of Information Science and Engineering, Hunan University, Changsha 410082, China

**Corresponding author: cjzhao@hun.edu.cn*

Received November 20, 2013; accepted January 15, 2014; posted online February 28, 2014

Based on the coupled Ginzburg-Landu equation, we numerically investigate the pulse dynamics in a dispersion-managed normal dispersion Tm-doped mode-locked fiber laser. The influences of the modulation depth and saturation power of saturable absorber on the pulse dynamics are presented. The simulation results show that these parameters are crucial to achieve high pulse energy and high pulse peak power pulsed laser near 2-μm wavelength.

OCIS codes: 140.3510, 320.7090, 190.4370.

doi: 10.3788/COL201412.031405.

High power, ultra-short fiber lasers operating near 2 μm have attracted much attention because their wide range of application in light detection and ranging (LIDAR), optical communication, spectroscopy, and efficient attainment of mid-infrared laser[1−4]. Among all the options, passive mode-locked Tm-doped fiber lasers operating in the range of 1800−2100 nm is one of the most prevalent ones[5−7]. Moreover, energy scaling in mode-locked fiber lasers depends strongly on the cavity dispersion management[8−12], and in particular in the normal dispersion regime[13−15].

To construct a mode-locked fiber laser, saturable absorber plays a key role in stabilizing and shortening mode-locked fiber laser. Therefore, how to select the saturable absorber (SA) and control its parameters are very important[16,17]. Semiconductor saturable absorber mirrors (SESAMs) was considered as one of the most successful passive mode-locker[18]. However, SESAMs have relatively narrow operation bandwidth, usually a few tens nm, and their parameters are not easy to control. With the development of novel SAs, such as carbon nanotube (CNT) and graphene, controlling the SA parameter becomes relatively easy[19−21]. For example, the modulation depth and saturable power of graphene can just be tuned by varying the thickness of graphene film[22]. Recently, a novel saturable absorber with high modulation depth, topological insulator, has been studied[23]. It is expected that these saturable absorbers will make a big difference for laser performance compared with conventional saturable absorber. Therefore, studying the SA parameters in the fiber oscillator numerically may be beneficial as well as it allows of investigating a wide range of independent SA parameters, which would be difficult to perform in experiments. In this letter, we numerically investigated the effect of saturation absorber parameters on the pulse dynamics of the normal dispersion Tm-doped fiber laser. A dispersion managed normal dispersion cavity is modeled which is useful to generate high power and ultra-short pulse output.

The proposed dispersion-managed normal dispersion Tm-doped fiber laser is schematically shown in Fig. 1. The oscillator is made up of a wavelength-division multiplexing (WDM) coupler, an isolator, a polarization controller (PC), an output coupler (OC), a fast saturable absorber (SA), and three segments of fiber. The total length of the laser cavity is 6.9 m, including a 3-m-long passive single-mode fiber (SMF-28e), a 1.0-m-Tm-doped gain fiber. To make dispersion management at 2 μm wavelength is not easy because standard single mode fibers (SMF) at 1 and 1.5 μm exhibit large anomalous dispersion at 2-μm. Here, a 2.9-m-long high numerical aperture SMF with large normal dispersion at 2 μm used for dispersion compensation[24,25]. The unidirectional propagation of intracavity pulse is controlled by a polarization independent isolator.

The pulse propagation was modeled in the weakly birefringence fibers based on asymmetrical spit-step Fourier algorithm that solves the well-known coupled Ginzburg-Landu equation[26]:

$$\begin{aligned}\frac{\partial F_x}{\partial Z} =& j\frac{\Delta\beta}{2}F_x - \delta\frac{\partial F_x}{\partial T} - \beta_2\frac{j}{2}\frac{\partial^2 F_x}{\partial T^2} + \frac{\beta_3}{6}\frac{\partial^3 F_x}{\partial T^3} \\ &+ j\gamma\left(|F_x|^2 + \frac{2}{3}|F_y|^2\right)F_x + j\frac{\gamma}{3}F_x^* F_y^2 \\ &+ \frac{g}{2}F_x + \frac{g}{2Bw}\cdot\frac{\partial F_x^2}{\partial T^2},\end{aligned} \tag{1}$$

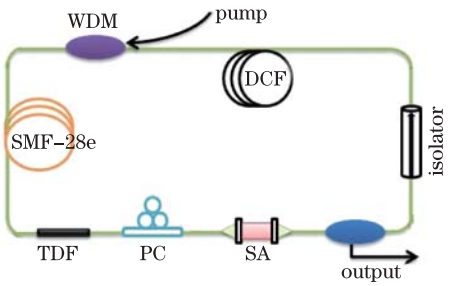

Fig. 1. Dispersion-managed normal dispersion Tm-doped fiber laser. TDF: Tm-doped fiber; DCF: dispersion compensation fiber.

$$\frac{\partial F_y}{\partial Z} = -j\frac{\Delta\beta}{2}F_y + \delta\frac{\partial F_y}{\partial T} - \beta_2\frac{j}{2}\frac{\partial^2 F_y}{\partial T^2} + \frac{\beta_3}{6}\frac{\partial^3 F_y}{\partial T^3} + j\gamma\left(|F_y|^2 + \frac{2}{3}|F_x|^2\right)F_y + j\frac{\gamma}{3}F_y^* F_x^2 + \frac{g}{2}F_y + \frac{g}{2Bw}\cdot\frac{\partial F_y^2}{\partial T^2}, \quad (2)$$

where F_x and F_y are the slowly varying amplitude envelopes of pulse along the two orthogonal polarized modes of the optical fiber, Z is the propagation coordinate, T is the time scale to the pulse duration, $\Delta\beta$=$2\pi/L_b$ is the wave-number difference between the two modes and L_b=$\lambda_0/\Delta n$ is the beat length, γ is the nonlinear coefficient of the fibers, parameter β_2 and β_3 are the two order dispersion coefficient and third order dispersion coefficient of the fibers, respectively. $B_{\rm w} = \Omega_g^2$ and Ω_g is the gain bandwidth, and parameter g represents the saturation gain coefficient of the gain fiber which can be described as

$$g = g_0/(1 + E_{\rm pulse}/E_{\rm sat}). \quad (3)$$

Here, g_0 is the small signal gain which taken as $\sim$ 30 dB; $E_{\rm sat}$ is the gain saturation energy which depends on pump power.

In this cavity configuration, an ideal fast SA is used for initializing mode-locked and it can be given by a function of transmission T[27]:

$$T = 1 - q_0/(1 + P/P_{\rm sat}), \quad (4)$$

where q_0 is the modulation depth of the SA , and $P_{\rm sat}$ is the saturation power of the SA.

In our simulation, we neglect the effect of the loss and third dispersion of the fibers for simplicity. To make the simulation possibly close to the experimental situation, we used the following parameters: SMF-28e, β_2= –60 ps^2/km, γ=4.7 W^{-1}km^{-1}; TDF, β_2= –80 ps^2/km, γ=5.8 W^{-1}km^{-1}; DCF, β_2= +90 ps^2/km, γ=5 W^{-1}km^{-1}; $E_{\rm sat}$=5 nJ, λ_0=2000 nm, L_b=100 m. The net cavity dispersion is 0.001 ps^2 which calculated by $\beta_2^{\rm net} = \beta_2^{\rm SMF-28e}\cdot L_{\rm SMF-28e} + \beta_2^{\rm TDF}\cdot L_{\rm TDF} + \beta_2^{\rm DCF}\cdot L_{\rm DCF}$.

We assumed initial field is a Gaussian pulse, and numerically, we find that stable soliton can be formed over a reasonably wide range of parameters. A typical soliton can be obtained with $P_{\rm sat}$=25 W, q_0=0.1, Ω_g=45 nm, OCR=0.1, as shown in Fig. 2. The pulse evolution with roundtrips without change of the total intensity indicates the soliton solution is stable (Fig. 2(a)). Figure 2(b) shows a significantly pulse evolution along all elements of the fiber laser over one cavity round-trip. A duration of 0.98-ps Gaussian shape pulse and an optical spectrum with characteristic steep spectral edge, as shown in Figs. 2(c) and (d), reveal that the soliton we obtained is a dissipative soliton in the normal dispersion region[10,11]. The quadratic spectral phase, i.e. the linear chirp, was calculated about 0.02 ps^2 for the pulse.

To investigate the influences of modulation depth of SA on pulse dynamics, numerical simulations were performed by varying the modulation depth from 0.1 to 0.6. By simulation, it can be found that when the modulation depth is greater than 0.6, the mode-locking operation becomes unstable. The reason may be explained by Eq. (4). For a constant $P_{\rm sat}$, modulation depth is inversely

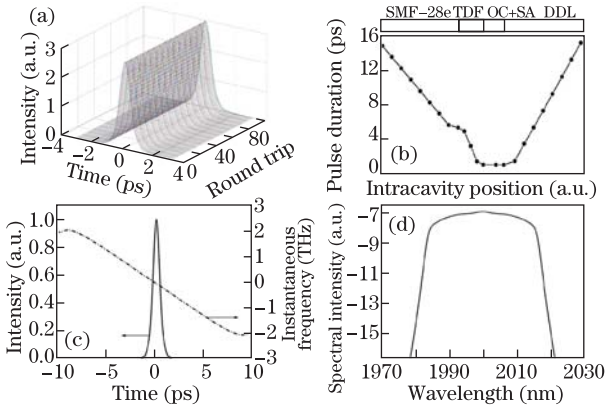

Fig. 2. Stable pulse output. (a) Pulse train; (b) pulse evolution of one roundtrip; (c) output single pulse and instantaneous frequency (dash-dotted curve); (d) spectrum (Log.scale).

proportional to transmission which means the higher modulation depth, the lower transmission, leading to more loss induced by SA. As a result, the total loss of the cavity is unable to balance the gain, which makes the mode-locking unstable.

The intracavity pulse dynamics and output pulse characteristics as the function of the modulation depth are summarized in Fig. 3. Figure 3(a) shows the intracavity evolution of the temporal pulse width under different modulation depths versus intracavity position. Similar to that of Ref. [16], the pulse width decreases along the negative dispersion fibers (SMF-28e and TDF), while broadening gradually after pulse evolves in the positive dispersion fiber. It is worth noting that the relative fluctuation of pulse width during intracavity propagation is greater than that of Ref. [16]. Considering the fiber laser operating in the nero-zero normal dispersion region, the result may be possible. The corresponding pulse spectral full-width at half-maximum (FWHM) evolution dynamics of intracavity are exhibited in Fig. 3(b), by which we can obtain that the spectral FWHM varied dramatically at the part of gain fiber and OC. The evolution of pulse energy for single pulse is shown in Fig. 3(c). Comparing the pulse energy dynamics in the three cases of modulation depth, a much higher energy can be achieved at low modulation depth. In addition, as we can see in Fig. 3(c), the difference of pulse energy between arbitrary two cases of modulation depth is large, which indicates that it is essential to control modulation depth of some materials used as SA elaborately in our realistic experiment. Figure 3(d) is the output spectrum with the modulation depth varying from 0.1 to 0.4, and the steep spectral edge are losing gradually which may attribute to the reduction of frequency chirp. The properties of output pulse are plotted in Fig. 3(e), where pulse width, spectral FWHM, and pulse energy decrease gradually with the increase of modulation depth. Moreover, with high modulation depth (q_0 >0.4), the pulse width almost keep constant. Furthermore, the increasing modulation depth results in the decreasing pulse width and spectral width. The reason may be that under the condition of fixed pump power, higher modulation depth means more loss, leading to the decrease of intracavity pulse peak power and nonlinear phase shift diminution, i.e., frequency chirp is reduced.

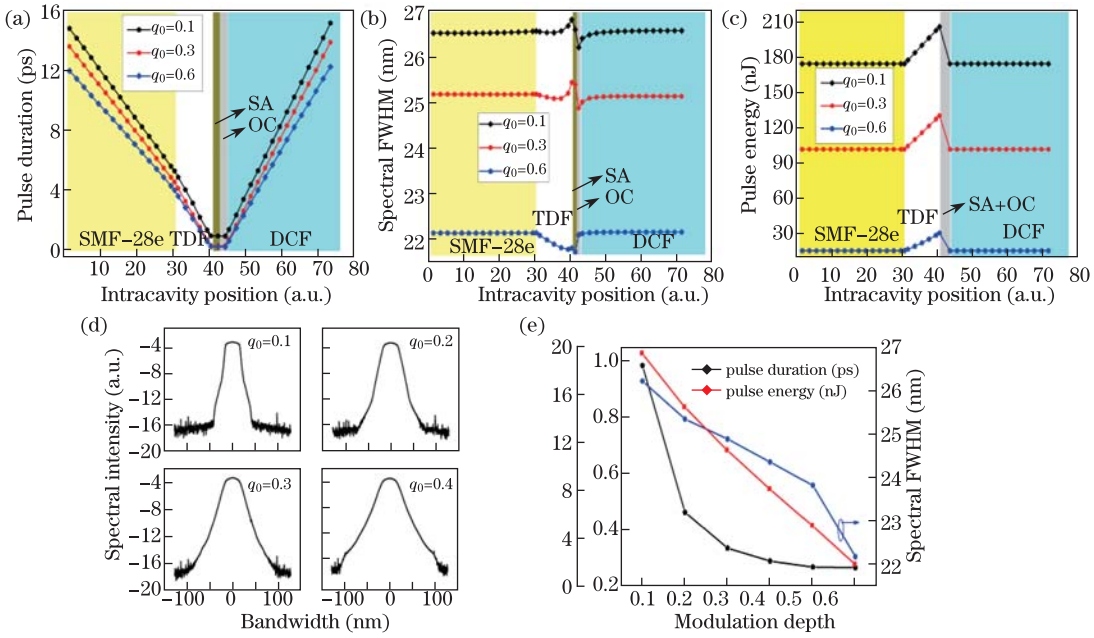

Fig. 3. Intracavity pulse evolution for (a) pulse duration, (b) spectral FWHM, and (c) energy with different modulation depths. (d) Output spectra (Log. Scale) at different modulation depths; (e) output pulse properties as a function of modulation depth.

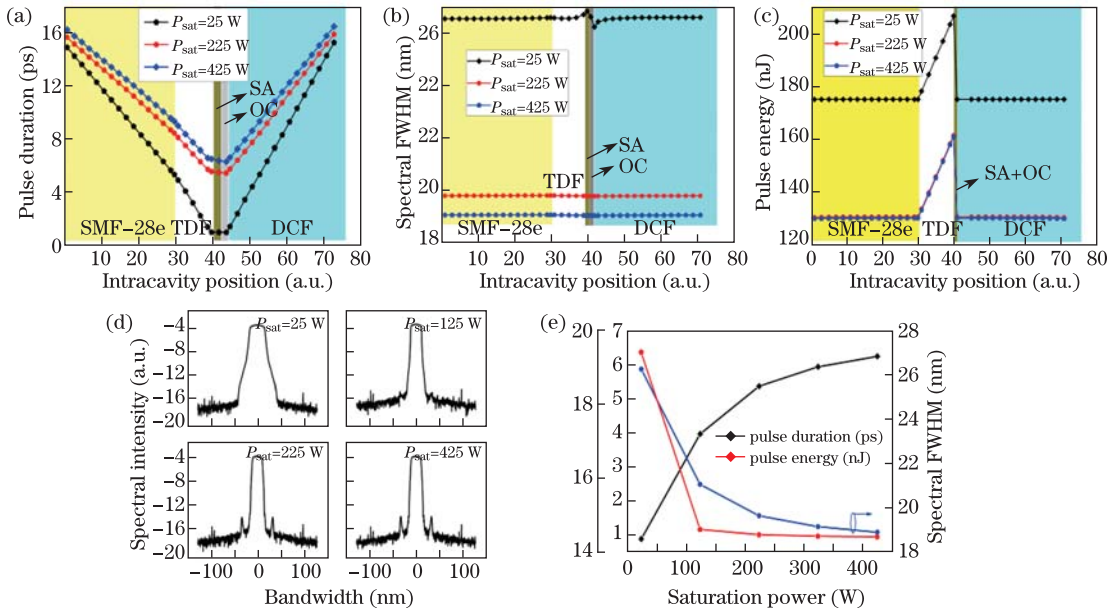

Fig. 4. Intracavity pulse evolution for (a) pulse duration, (b) spectral FWHM, and (c) energy with different saturation powers. (d) Output spectra (Log.Scale) at different saturation powers; (e) output pulse properties as a function of saturation power.

Another parameter of SA that can affect the laser intracavity pulse dynamics and output performance is the saturation power. In order to fully understand the effect of the saturation power of SA, numerical simulations were performed with the similar parameters as that in Fig. 2, as illustrated in Fig. 4.

The evolution in the intracavity position of temporal pulse width and pulse energy are similar to the results we previously obtained with different modulation depths, as shown in Figs. 4(a) and (c), respectively. One can observe from Figs. 4(a) and (c) that the pulse width is proportional to saturation power whereas the relation between pulse energy and saturation power is inversely proportional. Furthermore, when $P_{\rm sat}$ >200 W, the pulse energy nearly keep constant as saturation power increases although pulse width is broadened remarkably. Figure 4(b) shows the output pulse spectral FWHM with the saturation power varies from 25 to 425 W, and we can obtain that the FWHM nearly keep constant along the cavity at the condition of $P_{\rm sat}$ >200 W. The variation of output spectrum with saturation power varies are plotted in Fig. 4(d), it obviously shows that, at high saturation

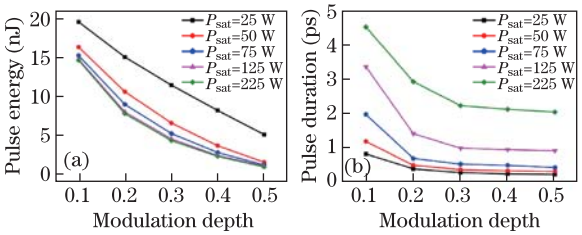

Fig. 5. (a) Output pulse energy and (b) pulse durations with different modulation depths at different saturation powers.

power, the spectrum becomes more narrower and steeper. The dependence of output pulse width, spectral FWHM and pulse energy on saturation power are shown in Fig. 4(e). It shows that the higher pulse energy and a narrower pulse width can be obtained at low saturation power.

In order to give a clear picture of the influences of SA parameters on the laser output characteristics, some simulations were performed with different saturation power at different modulation depth, as illustrated in Fig. 5. Figure 5(a) shows the output pulse energy at different saturation power with the modulation depth varying from 0.1 to 0.5. With the increased modulation depth, output pulse energies decrease. Moreover, for a given modulation depth, higher saturation power results in a lower pulse energy. It also can be seen that if the output pulse energy is held constantly, the higher modulation depth corresponds to lower saturable power. It is interesting to note that when the saturable power exceeds 125 W, the pulse energy changed little, which means that when the saturation power is higher enough, modulation depth becomes the key parameter to determine the output pulse energy. The relationship between output pulse width and modulation depth at different saturation powers are plotted in Fig. 5(b). It obviously shows that the narrower pulse can be obtained using SA with low saturation power and high modulation depth. Moreover, the pulse duration varies little when modulation depth is greater than 0.3.

In conclusion, the pulse dynamics in a dispersion-managed normal dispersion fiber laser cavity determined by modulation depth and saturation power of SA are systemically studied. It is verified that the SA parameters dramatically influence the properties of the Tm-doped dispersion-management fiber laser. Particularly, the variations of modulation depth lead to obvious pulse energy and pulse duration change. The simulation results in our work may provide guidelines for the optimization to obtain ultra-short pulse output in the high power and ultra-short Tm-doped fiber lasers.

This work was supported by the National Natural Science Foundation of China (No. 61205125) and the Fundamental Research Funds for the Central Universities.

References

1. M. E. Fermann and I. Hartl, Nat. Photon. **7**, 868 (2013).
2. S. D. Jackson, Nat. Photon. **6**, 423 (2012).
3. H. Lü, P. Zhou, H. Xiao, X. Wang, and Z. Jiang, Chin. Opt. Lett. **10,** 051403 (2012).
4. C. Guo, D. Shen, J. Long, and F. Wang, Chin. Opt. Lett. **10,** 091406 (2012).
5. M. A. Solodyankin, E. D. Obraztsova, A. S. Lobach, A. I. Chernov, A. V. Tausenev, V. I. Konov, and E. M. Dianov, Opt. Lett. **33,** 1336 (2008).
6. L. E. Nelson, E. P. Ippen, and H. A. Haus, Appl. Phys. Lett. **67,** 19 (1995).
7. Q. Wang, J. Geng, Z. Jiang, T. Luo, and S. Jiang, IEEE Photon. Technol. Lett. **23,** 682 (2011).
8. L. E. Nelson, D. J. Jones, K. Tamura, H. A. Haus, and E. P. Ippen, Appl. Phys. B **65,** 277 (1997).
9. F. ö. Ilday, J. R. Buckley, W. G. Clark, and F. W. Wise, Phys. Rev. Lett. **92,** 213902 (2004).
10. A. Chong, J. Buckley, W. Remomger, and F. Wise, Opt. Express **14,** 10095 (2006).
11. L. Zhao, D. Tang, H. Zhang, T. Cheng, H. Y. Tam, and C. Lu, Opt. Lett. **32,** 1806 (2007).
12. S. Kobtsev, S. Kukarin, and Y. Fedotov, Opt. Express **16,** 21936 (2008).
13. A. Wienke, F. Haxsen, D. Wandt, U. Morgner, J. Neumann, and D. Kracht, Opt. Lett. **37,** 2466 (2012).
14. F. Haxsen, D. Wandt, U. Morgner, J. Neumann, and D. Kracht, Opt. Express **18,** 18981 (2010).
15. W. H. Renninger, A. Chong, and F. W. Wise, IEEE J. Sel. Top. Quantum Electron. **18,** 289 (2012).
16. A. Cabasse, G. Martel, and J. L. Oudar, Opt. Express **17,** 9537 (2009).
17. Á. Szabó and Z. Várallyay, IEEE Photon. Technol. Lett. **24,** 122 (2012).
18. G. R. Jacobovitz–Veselka, U. Keller, and M. T. Asom, Opt. Lett. **17,** 1791 (1992).
19. H. Zhang, D. Tang, L. Zhao, Q. Bao, K. P. Loh, B. Lin, and S. C. Tjin, Laser Phys. Lett. **7**5, 91 (2010).
20. N. Nishizawa, Y. Seno, K. Sumimura, Y. Sakakibara, E. Itoga, H. Kataura, and K. Itoh, Opt. Express **16,** 9429 (2008).
21. A. Martinez and Z. P. Sun, Nat. Photon. **7**, 842 (2013).
22. Q. Bao, H. Zhang, Y. Wang, Z. Ni, Y. Yan, Z. Shen, K. P. Loh, and D. Tang, Adv. Funct. Mater. **19,** 3077 (2009).
23. C. Zhao, H. Zhang, X. Qi, Y. Chen, Z. Wang, S. Wen, and D. Tang, Appl. Phys. Lett. **101**, 211106 (2012).
24. Y. An, D. Shen, W. Zhao, and J. Long, Opt. Commun. **285,** 1949 (2012).
25. H. Liu, K. Kieu, S. Lefrancois, W. H. Renninger, A. Chong, and F. W. Wise, in *Proceeding of CLEO*: *Science and Innovations*, *Optical Society of America* (2011).
26. H. Zhang, D. Tang, L. Zhao, X. Wu, and H. Y. Tam, Opt. Express **17,** 455 (2009).
27. F. X. Kärtner, J. A. der Au, and U. Keller, IEEE J. Sel. Top. Quantum Electron. **4,** 159 (1998).